RESEARCH ARTICLE

A systems-level model reveals that 1,2-Propanediol utilization microcompartments enhance pathway flux through intermediate sequestration

Christopher M. Jakobson[1¤], Danielle Tullman-Ercek[1], Marilyn F. Slininger[2], Niall M. Mangan[3]*

1 Department of Chemical and Biological Engineering, Northwestern University, Evanston, IL, USA,
2 Department of Chemical and Biomolecular Engineering, University of California, Berkeley, Berkeley, CA, USA, **3** Department of Applied Mathematics, University of Washington, Seattle, WA, USA

¤ Current address: Department of Chemical and Systems Biology, Stanford University, Stanford, CA, USA
* niallmm@gmail.com

Abstract

The spatial organization of metabolism is common to all domains of life. Enteric and other bacteria use subcellular organelles known as bacterial microcompartments to spatially organize the metabolism of pathogenicity-relevant carbon sources, such as 1,2-propanediol. The organelles are thought to sequester a private cofactor pool, minimize the effects of toxic intermediates, and enhance flux through the encapsulated metabolic pathways. We develop a mathematical model of the function of the 1,2-propanediol utilization microcompartment of *Salmonella enterica* and use it to analyze the function of the microcompartment organelles in detail. Our model makes accurate estimates of doubling times based on an optimized compartment shell permeability determined by maximizing metabolic flux in the model. The compartments function primarily to decouple cytosolic intermediate concentrations from the concentrations in the microcompartment, allowing significant enhancement in pathway flux by the generation of large concentration gradients across the microcompartment shell. We find that selective permeability of the microcompartment shell is not absolutely necessary, but is often beneficial in establishing this intermediate-trapping function. Our findings also implicate active transport of the 1,2-propanediol substrate under conditions of low external substrate concentration, and we present a mathematical bound, in terms of external 1,2-propanediol substrate concentration and diffusive rates, on when active transport of the substrate is advantageous. By allowing us to predict experimentally inaccessible aspects of microcompartment function, such as intra-microcompartment metabolite concentrations, our model presents avenues for future research and underscores the importance of carefully considering changes in external metabolite concentrations and other conditions during batch cultures. Our results also suggest that the encapsulation of heterologous pathways in bacterial microcompartments might yield significant benefits for pathway flux, as well as for toxicity mitigation.

Author Summary

Many bacterial species, such as *Salmonella enterica* (responsible for over 1 million illnesses per year in the United States) and *Yersinia pestis* (the causative agent of bubonic plague), have a suite of unique metabolic capabilities allowing them to proliferate in the hostile environment of the host gut. Bacterial microcompartments are the subcellular organelles that contain the enzymes responsible for these special metabolic pathways. In this study, we use a mathematical model to explore the possible reasons why *Salmonella* enclose the 1,2-propanediol utilization metabolic pathway within these sophisticated organelle structures. Using our model, we can examine experimentally inaccessible aspects of the system and make predictions to be tested in future experiments. The metabolic benefits that bacteria gain from the microcompartment system may also prove helpful in enhancing bacterial production of fuels, pharmaceuticals, and specialty chemicals.

Introduction

Bacterial microcompartments (MCPs) are protein-bound intracellular organelles used by *Salmonella enterica*, *Yersinia pestis*, *Klebsiella* spp., and other bacteria to spatially organize their metabolism [1–3]. MCP metabolons allow the growth of these pathogens on carbon and energy sources, such as 1,2-propanediol [4] and ethanolamine [5], that confer a competitive advantage upon invasion of the host gut [6–10]. MCPs are typically approximately 150 nm in diameter, with multiple enzymes localized inside a porous, monolayer shell composed of several distinct proteins [4, 11, 12]; a typical bacterial cell contains several MCP structures when in the presence of the appropriate substrate. Enzymes are localized to the MCP interior through the interactions of N-terminal signal sequences with the inward-facing helices of MCP shell proteins, and potentially through other uncharacterized interactions [13–15].

Inside the 1,2-propanediol utilization (Pdu) MCP metabolon, 1,2-propanediol metabolism proceeds as follows: the vitamin B_{12}-dependent PduCDE holoenzyme converts 1,2-propanediol to propionaldehyde [14], then propionaldehyde is converted to either 1-propanol by the NADH-dependent PduQ enzyme [16] or to propionyl-coA by the NAD^+-dependent PduP enzyme [17] (Fig 1A). The PduP and PduQ enzymes are thought to cycle a private pool of NAD^+/NADH inside the MCP lumen, enforcing a 1-to-1 stoichiometry for the two reactions. This assumption is reinforced by experimental observations that mutants defective in one of these genes are not rescued by the cytosolic production of homologues [16, 18, 19]. 1-propanol is not used for cell growth in the presence of 1,2-PD, but propionyl-CoA can be utilized either as a carbon source or for ATP generation through substrate-level phosphorylation [20]. For the purposes of this model, we neglect the downstream products and any effects their concentrations might have on the rates of catalysis by PduCDE and PduP/Q, as there is limited experimental evidence in this regard.

Pdu MCPs are elaborate multi-protein structures subject to exquisite regulation, and much investigation has focused on determining the detailed function of the organelles. Experiments suggest that metabolic pathways are sequestered in the Pdu and ethanolamine utilization (Eut) MCPs in order to protect the cell from toxicity associated with aldehyde intermediates [21], to prevent carbon loss from the metabolic pathway [19], and to provide a private pool of cofactors for the encapsulated pathways [18, 19]. These mechanistic hypotheses are difficult to confirm experimentally, as directly measuring the concentrations of small molecules inside the MCPs *in vivo* remains a challenge. Here we build a coupled reaction-diffusion model of the Pdu
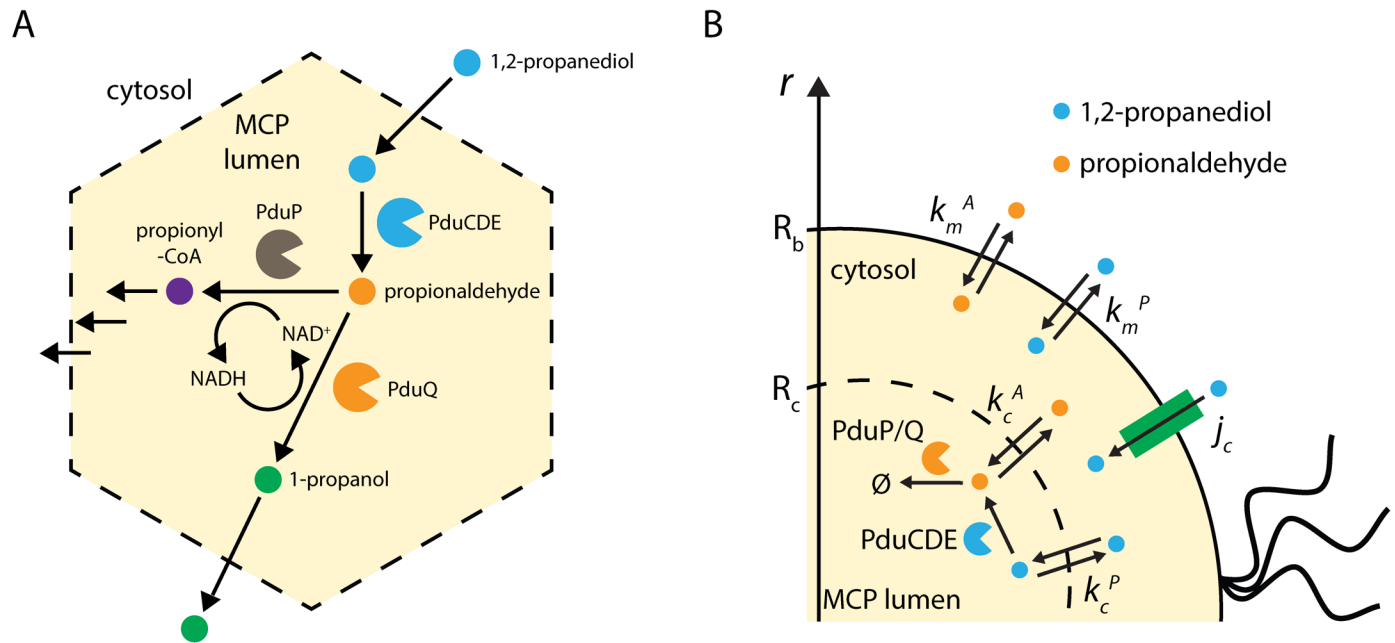
Fig 1. Reaction schemes. Reaction scheme for (A) the native Pdu MCP and (B) the simplified model considered here.

MCP and use computational and analytic approaches to assess whether the described biological system produces the hypothesized mechanistic behavior. The use of a mechanistic model of the MCP allows us to examine potential functions and behavior across a wide range of parameters, providing a framework for incorporating experimental observations and guiding experimental design.

The model presented here follows an approach used to investigate the function of a related organelle, carboxysomes, in the CO_2 concentrating mechanism of cyanobacteria [22]. Modeling of the cyanobacterial system indicated that the carboxysome can significantly increase carboxylation efficiency by reducing the rate of unproductive oxygenation by RuBisCO. The Pdu MCP, however, differs in critical respects. The first reaction in the model of carboxysome metabolism, catalyzed by carbonic anhydrase, is reversible; the reaction catalyzed by PduCDE, in contrast, is effectively irreversible. Secondly, the Pdu MCP may play two roles, toxicity mitigation and flux enhancement, while the carboxysome does not function to sequester a toxic intermediate. The relative importance of these two functions is unclear *a priori*, and the modeling approach herein allows us to examine the possible trade-offs between the two.

For simplicity, we model the Pdu MCP as a spherical compartment in the center of a radially symmetric spherical cell. The model includes passive transport of 1,2-PD and propionaldehyde across the cell membranes and MCP shell, possible active transport of 1,2-PD into the cell, and the action of the PduCDE and PduP/Q enzymes localized within the MCP (Fig 1B). Parameters were estimated *a priori* or based on experimental results. We have developed a numerical simulation for this spherical geometry with localization of enzymes to the MCP. By making the assumption of constant metabolite concentrations in the MCP lumen, we have also developed a closed-form analytic solution that well approximates the full numerical solution for a broad range of physically relevant parameter values (S1 Fig; see also Models). The

analytic approximation allows for explicit examination of the relationships between different parameters and the mechanisms in the system. This analytical solution is used throughout the following analysis.

We find that aldehyde sequestration is the key function of the Pdu MCP, and contributes not only to decreasing aldehyde leakage into the cytosol and the growth medium, as is often discussed in the existing literature [21], but also to greatly increasing flux through the metabolon by increasing the substrate concentration in the vicinity of the relevant enzymes. Furthermore, we find that active 1,2-PD transport across the cell membrane is dispensable at some external 1,2-PD concentrations, including the concentrations at which most laboratory experiments are performed, but not at low external 1,2-PD concentrations. This transport activity has been proposed previously, but never experimentally observed [25]. Finally, while selective MCP membrane permeability is not always required to achieve optimal substrate concentrations, it is often advantageous in this regard. The qualitative behavior of our model and quantitative fluxes and metabolite concentrations agree well with existing experimental results, without fitting any model parameters to experimental data (the MCP shell permeability is optimized to maximize flux, but is not fit to data). Additionally, our results suggest several avenues for continuing computational and experimental investigation, including investigations into 1,2-PD active transport, direct characterization and detailed simulation of MCP membrane permeability, and analysis of MCP function in chemostatic cultures.

Models

We model Pdu MCP function using a simple spatially resolved reaction-diffusion model incorporating passive and active transport across the cell membrane, passive transport across the MCP shell, and enzymatic catalysis of two critical steps in 1,2-propanediol metabolism: conversion of 1,2-propanediol to propionaldehyde by the PduCDE holoenzyme [9], and subsequent conversion of propionaldehyde to downstream products by the PduP and PduQ enzymes [11, 12]. We model the bacterial cell as a spherical compartment of radius 500 nm, containing at its center a single spherical MCP of radius 100 nm (representing the same fraction of the cell volume as 5 Pdu MCPs in a typical bacterial cell; Fig 1B).

The key assumptions in the model are as follows:

1. we assume that the cell and the MCP are spherically symmetrical, such that $f(r, \theta, \phi) = f(r)$ only, and $\nabla^2 f = \frac{1}{r^2} \frac{\partial}{\partial r} \left(r^2 \frac{\partial f}{\partial r} \right)$;

2. we consider the system at steady state;

3. we consider constant external concentrations of 1,2-propanediol (P_{out}) and propionaldehyde (A_{out});

4. and we assume that the enzyme-catalyzed reactions are irreversible, and neglect reactions downstream of PduP/Q.

We assume that the conversion of P to A in the absence of enzymatic catalysis is negligible, so the equations for diffusion of 1,2-PD, P, and propionaldehyde, A, in the cytosol are as follows:

$$D\nabla^2 P(r) = 0. \tag{1}$$

$$D\nabla^2 A(r) = 0 \tag{2}$$

Where D is the diffusion coefficient of the metabolites in the cytosol.

The analogous equations in the MCP are:

$$D\nabla^2 P_{MCP}(r) - R_{CDE}(P_{MCP}(r)) = 0 \tag{3}$$

$$D\nabla^2 A_{MCP}(r) + R_{CDE}(P_{MCP}(r)) - R_{PQ}(A_{MCP}(r)) = 0 \tag{4}$$

Inside the Pdu MCP, we assume Michaelis-Menten kinetic behavior of the PduCDE and PduP/PduQ enzymes, so the equation for the rate of the PduCDE (diol dehydratase) reaction is

$$R_{CDE}(P_{MCP}(r)) = \frac{V_{CDE}P_{MCP}(r)}{K_{MCDE} + P_{MCP}(r)} \tag{5}$$

Here V_{CDE} is the maximum rate of dehydration by PduCDE. K_{MCDE} is the half maximum concentration for dehydration.

PduP and PduQ are redox-coupled by the cycling of NAD+/NADH, so we assume that their catalytic rates are equal at steady state; the equation for the PduP and PduQ reactions is therefore:

$$R_{PQ}(A_{MCP}(r)) = \frac{2V_{PQ}A_{MCP}(r)}{K_{MPQ} + A_{MCP}(r)} \tag{6}$$

Here V_{PQ} is the maximum rate of aldehyde consumption by PduP, and K_{MPQ} is the half maximum concentration. The rate is doubled due to cofactor cycling to yield the rate of PduP/Q combined.

We assume that P and A are transported across the cell membranes by passive diffusion, so we can specify the following boundary conditions enforcing continuity of flux of each metabolite at the cell membrane. We neglect the effect of small molecule concentrations on membrane permeability, as there is no experimental evidence in this regard for propionaldehyde or 1,2-PD. In addition to passive diffusion across the cell membrane, we also include the possibility of active transport of P across the cell membrane by the putative membrane protein encoded by *pduF*.

$$D\frac{\partial P}{\partial r}\Big|_{r=R_b} = j_c P_{out} + k_m^P\left(P_{out} - P_{cytosol}(r = R_b)\right) \tag{7}$$

$$D\frac{\partial A}{\partial r}\Big|_{r=R_b} = k_m^A\left(A_{out} - A_{cytosol}(r = R_b)\right) \tag{8}$$

Here active transport of P is set by the transport velocity j_c. The permeabilities of the cell membrane to A and P are set by the diffusive velocities k_m^A and k_m^P.

The passive transport velocities of P and A across the MCP shell can be treated independently or as being equal; we explore the necessity of selective permeability by allowing the velocities to differ. The boundary condition at the MCP shell sets the gradient at the shell as the difference in concentration between the cytosolic and MCP concentrations times the diffusive velocity:

$$D\frac{\partial P}{\partial r}\Big|_{r=R_c} = k_c^P(P_{cytosol}(r = R_c) - P_{MCP}(r = R_c)) \tag{9}$$

$$D\frac{\partial A}{\partial r}\Big|_{r=R_c} = k_c^A(A_{cytosol}(r = R_c) - A_{MCP}(r = R_c)) \tag{10}$$

Table 1. Parameter estimates used in our model.

Parameter	Meaning	Estimated Value	Units
j_c	Rate of active transport of 1,2-PD across the cell membrane	1 (when present) [22]	$\frac{cm}{s}$
k_c^A	Permeability of the Pdu MCP to propionaldehyde	10^{-5}	$\frac{cm}{s}$
k_c^P	Permeability of the Pdu MCP to 1,2-PD	10^{-5}	$\frac{cm}{s}$
R_b	Radius of the bacterial cell	$5x10^{-5}$	cm
R_c	Radius of the Pdu MCP	10^{-5} [12]	cm
D	Diffusivity of metabolites in the cellular milieu	10^{-5} [37]	$\frac{cm^2}{s}$
k_m^A	Permeability of the cell membrane to propionaldehyde	10^{-3} [38]	$\frac{cm}{s}$
k_m^P	Permeability of the cell membrane to 1,2-PD	10^{-3} [39]	$\frac{cm}{s}$
k_{catCDE}	Maximum reaction rate of a PduCDE active site	$3x10^2$ [39]	$\frac{1}{s}$
N_{CDE}	Number of PduCDE enzymes per cell	$1.5x10^3$ [12]	$\frac{1}{cell}$
K_{MCDE}	Michaelis-Menten constant of PduCDE	$5x10^2$ [39]	μM
k_{catPQ}	Maximum reaction rate of a PduPQE active site	55 [16]	$\frac{1}{s}$
K_{MPQ}	Michaelis-Menten constant of PduPQ	$1.5x10^4$ [16]	μM
N_{PQ}	Number of PduPQ enzymes per cell	$2.5x10^3$ [12]	$\frac{1}{cell}$
P_{out}	External 1,2-PD concentration	$5.5x10^4$ [21]	μM
A_{out}	External propionaldehyde concentration	0 [21]	μM

https://doi.org/10.1371/journal.pcbi.1005525.t001

We can obtain good estimates of most of the parameters from the literature, as shown in Table 1. The nonspecific permeability of the MCP k_c was chosen to maximize the flux through PduP/Q. Unless otherwise specified, the baseline estimates in Table 1 are used in all following analyses.

A sensitivity analysis of the total pathway flux with respect to each parameter is shown in S2 Fig; model sensitivity is shown both for the MCP and scaffold cases. It can be seen, for instance, that the predicted pathway flux is insensitive to perturbations in the external 1,2-PD concentration when the concentration is 55 mM, but not when the concentration is 0.5 mM (S2 Fig). The behavior of these local perturbations is in good agreement with the global behavior described in detail below.

Our estimates of the number of PduCDE and PduP/Q enzymes (N_{CDE} and N_{PQ}) are based on experimental observations of the abundance of Pdu MCP constituents in purified samples [12]. The effects of changes in the total number of enzymes ($N_{CDE} + N_{PQ}$) and in the relative ratio of the enzymes (holding the total number of enzymes constant) are shown in S3 Fig Interestingly, the optimal ratio of N_{CDE} to N_{PQ} predicted by the model is close to the experimentally observed value of this parameter, and is not inversely proportional to the maximum catalytic rates of each enzyme. $k_{catCDE} \approx 3x10^2$ and $k_{catPQ} \approx 55$, so a rate-matching argument would predict an optimal ratio of $\frac{N_{PQ}}{N_{total}} \approx 86\%$, but the model instead predicts (and experiments observe) that a ratio between 60% and 75% PduP/Q is optimal [12].

As is often the case in biological modeling, the parameters available in the literature (Table 1) are measured in a variety of experiments. Our approach mitigates the potential for parameter error by comprehensively varying the parameter values within several orders of magnitude defined by the physically reasonable range. This exploration allows us to map out the behavior of the system within a global parameter space, and the qualitative results are insensitive to the precise values of the initial parameters used.

Non-dimensional equations

We derive nondimensional equations which are then solved numerically by a finite-difference approach to find the steady-state concentrations in the MCP, and the solutions in the cytosol follow directly. We solve the spherical finite-difference equations using the `ODE15s` solver in MATLAB. Details of the non-dimensionalization can be found in S1 Text, and the corresponding MATLAB code can be found at https://github.com/cjakobson/pduMCPmodel.

Analytical solution

If we assume that the concentration gradients in the MCP are small, then the concentrations P_{MCP} and A_{MCP} are approximately constant and the full solution to the reaction-diffusion equations in the MCP and cytosol can be found analytically. This assumption is tantamount to assuming that the quantity $\xi = \frac{K_{MPQ}D}{V_{CDE}R_c^2} >> 1$ (see S1 Text); given our assumptions, we estimate that the value of ξ is approximately 10^4. The detailed solution is shown in S1 Text.

Equations for no MCP case

In the case when there is no Pdu MCP, we assume that the same number of enzymes are now distributed throughout the cell. We can thence derive nondimensional equations which can be solved numerically by a finite-difference approach as above (see S1 Text).

Results

MCPs reduce toxicity by decoupling cytosolic aldehyde concentration from PduP/Q saturation

In order to assess the function of the Pdu MCP, we compare the performance of the Pdu MCP system to two alternative organizational strategies for the Pdu metabolic enzymes: uniform distribution of the enzymes throughout the cytosol, and co-localization on a scaffold without a diffusion barrier. We assess the function of each organization strategy by two criteria: (i) maintenance of the cytosolic propionaldehyde concentration below the toxicity limit of 8 mM [21] in Fig 2A, and (ii) saturation of the PduP/Q enzymes with their propionaldehyde substrate in Fig 2B. Flux through the Pdu metabolon is maximized when the enzymes are saturated. In each organizational case, we examine the kinetically relevant propionaldehyde concentration (Fig 2B): without MCPs, this is the cytosolic propionaldehyde concentration; with MCPs, this is the propionaldehyde concentration in the MCP. In all cases, we initially neglect active transport of 1,2-PD at the cell membrane ($j_c = 0$).

The case of enzymes distributed throughout the cytosol provides an assessment of the baseline efficacy of the Pdu pathway without compartmentalization. As the Michaelis-Menten constant of the PduP/Q enzymes is approximately 15 mM, above the propionaldehyde toxicity limit, it is impossible to both saturate the PduP/Q enzymes and remain below the toxicity limit in the same location. In fact, if the PduCDE and PduP/Q enzymes are distributed throughout the cytosol, our model suggests that the steady-state propionaldehyde concentration is maintained at 2.4 μM (several orders of magnitude below the 8 mM toxicity limit) when the external propanediol concentration is 55 mM (Fig 2A, S4 Fig). In turn, the PduP/Q enzymes, with a K_M of 15 mM, are not saturated (Fig 2B).

Another organizational strategy is localization of the relevant enzymes to a scaffold, without a diffusion barrier. In this case, the propionaldehyde concentration in the vicinity of the PduP/Q enzymes is 2.8 μM, higher than if the enzymes are distributed throughout the cytosol (in
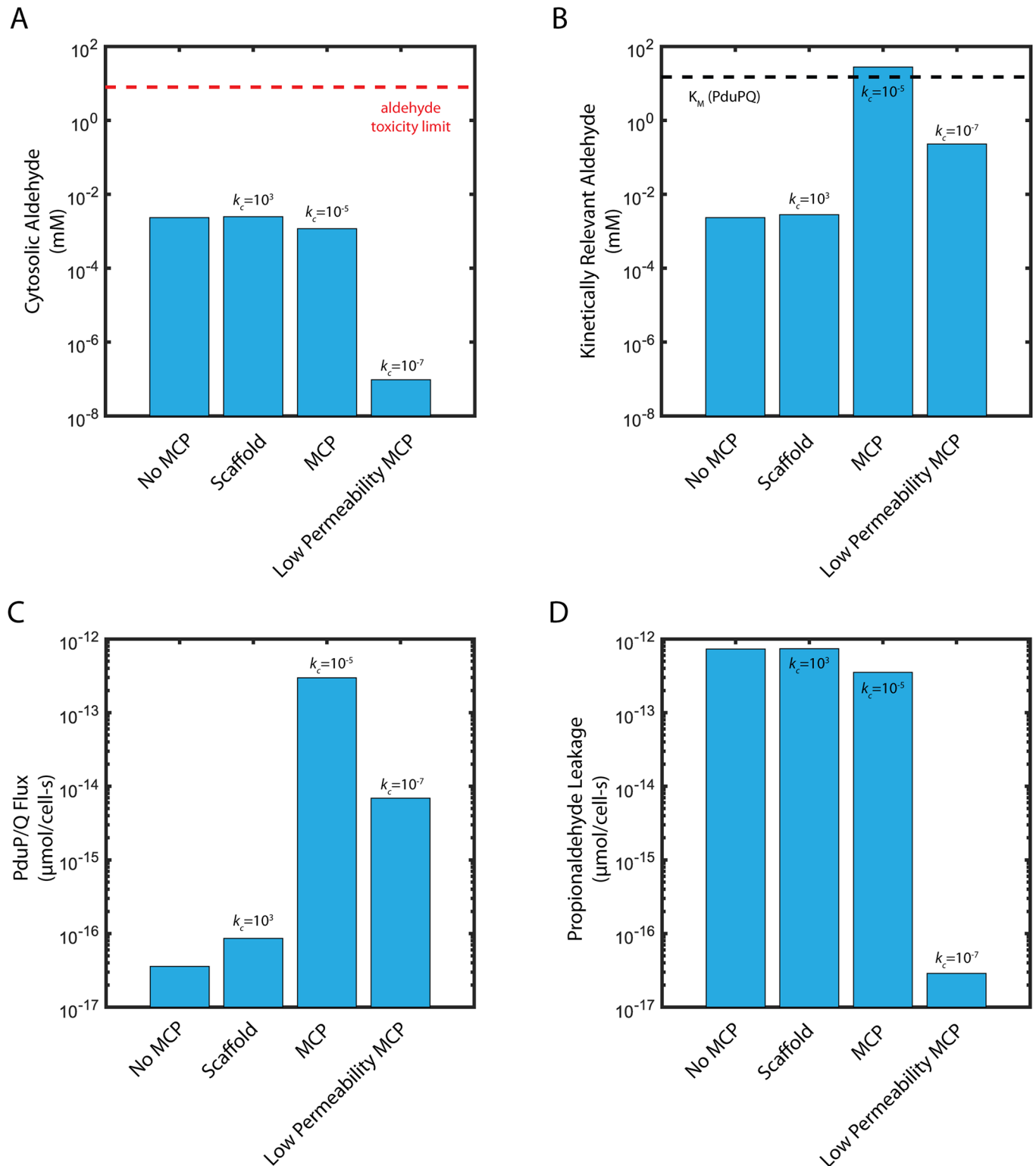
Fig 2. (A) Cytosolic propionaldehyde concentration (A_{cyto}), (B) kinetically relevant propionaldehyde concentration (A_{MCP} or A_{cyto}, as appropriate), (C) carbon flux through PduP/Q, and (D) propionaldehyde leakage out of the cell into the extracellular space. Shown are the steady state concentrations and propionaldehyde fluxes for cases without MCPs, with a scaffold, with MCPs, and with MCPs of extremely low permeability. The 15 mM K_M of PduP/Q is shown as a black dashed line in (B); the 8 mM propionaldehyde cellular toxicity limit is shown as a red dashed line in (A). Baseline parameters are in Table 1. Flux refers to the flux of propionaldehyde through conversion catalyzed by the PduP/Q enzymes.

https://doi.org/10.1371/journal.pcbi.1005525.g002

which case the kinetically relevant concentration is 2.4 μM), but still much lower than the saturating concentration of 15 mM (Fig 2B).

When the enzymes are localized in the MCP (permeability of 10^{-5} cm/s for 1,2-PD and propionaldehyde), the PduP/Q enzymes are exposed to a much higher propionaldehyde concentration of 28 mM (higher than the saturating concentration) (Fig 2B), while the propionaldehyde concentration in the cytosol is 1.2 μM (Fig 2A). The presence of a diffusion barrier allows the MCP to decouple the cytosolic propionaldehyde concentration (responsible for toxicity) from the kinetically relevant propionaldehyde concentration in the vicinity of the PduP/Q enzymes. Very low nonspecific permeabilities of the diffusion barrier are unfavorable, however: a MCP with very low permeability (10^{-7} cm/s for 1,2-PD and propionaldehyde) maintains a very low cytosolic propionaldehyde concentration of 1 pM, but also a low concentration of propionaldehyde in the MCP of 230 μM (Fig 2A and 2B).

Optimally permeable MCPs are an effective means of decoupling a potentially toxic cytosolic aldehyde concentration from the kinetically relevant aldehyde concentration inside the MCP. PduP/Q saturation could also be achieved with a very low cell membrane permeability to propionaldehyde, causing an accumulation of propionaldehyde in the cytosol, but at the cost of cytosolic aldehyde concentrations above the toxicity limit (S5 Fig). In addition, the membrane permeability to propionaldehyde required for this to occur (10^{-7} cm/s) is dramatically lower than a physiologically reasonable estimate (10^{-3} cm/s).

MCPs enhance pathway flux

Decoupling PduP/Q saturation from cytosolic propionaldehyde concentration by encapsulation allows significantly greater carbon flux through the MCP metabolon than in the cases of enzyme scaffolding or no organization (Fig 2C). The flux of propionaldehyde per cell through PduP/Q in the MCP case ($2.97x10^{-13}$ μmol/cell-s) is four orders of magnitude higher than in either the scaffold or no MCP cases ($8.61x10^{-17}$ μmol/cell-s and $3.58x10^{-17}$ μmol/cell-s, respectively). Interestingly, this improvement is due solely to saturation of the PduP/Q enzymes; the flux through the PduCDE enzyme is similar with MCPs ($6.49x10^{-13}$ μmol/cell-s) and without ($7.41x10^{-13}$ μmol/cell-s). PduCDE production of aldehyde is sufficient in all four organizational cases, but without a substantial diffusion barrier in the form of the MCP shell, the aldehyde leaks into the cytosol or the extracellular space before it can be utilized by the PduP/Q enzymes.

To quantitatively evaluate our model we estimate the growth rate resulting from the predicted flux through PduP/Q in the MCP case. Most parameter estimates were made from literature or a priori (Table 1); the nonspecific MCP membrane permeability k_c was set to the value that resulted in the greatest flux through the PduP/Q enzymes in our model (Fig 3A). Again, we initially neglect active transport ($j_c = 0$). Our model predicts a flux of $2.97x10^{-13}$ μmol/cell-s for a cell with MCPs, equivalent to $1.74x10^{-5}$ pg/cell-s, when the external 1,2-PD concentration is 55 mM. Approximately one-half of this flux can be used for cell growth, since 1-propanol is excreted and not used for metabolism in the presence of 1,2-PD, so assuming that a bacterial cell has a dry weight of approximately 0.3 pg [23], our model predicts a time of approximately 9 hours for a cell with MCPs to metabolize enough biomass through the Pdu MCP metabolon to accumulate the mass of one daughter cell (Fig 3B). This value is in good agreement with experimentally measured doubling times for the growth of *Salmonella enterica* on 55 mM 1,2-PD of approximately 5-10 hours [21]. We believe the model is well suited to address batchwise experimental results of this kind because a typical experiment measuring the growth of *Salmonella* on 1,2-PD takes place over tens of hours, while our model has characteristic timescales on the order of seconds, at maximum (Table 2). The separation of time scales allows us
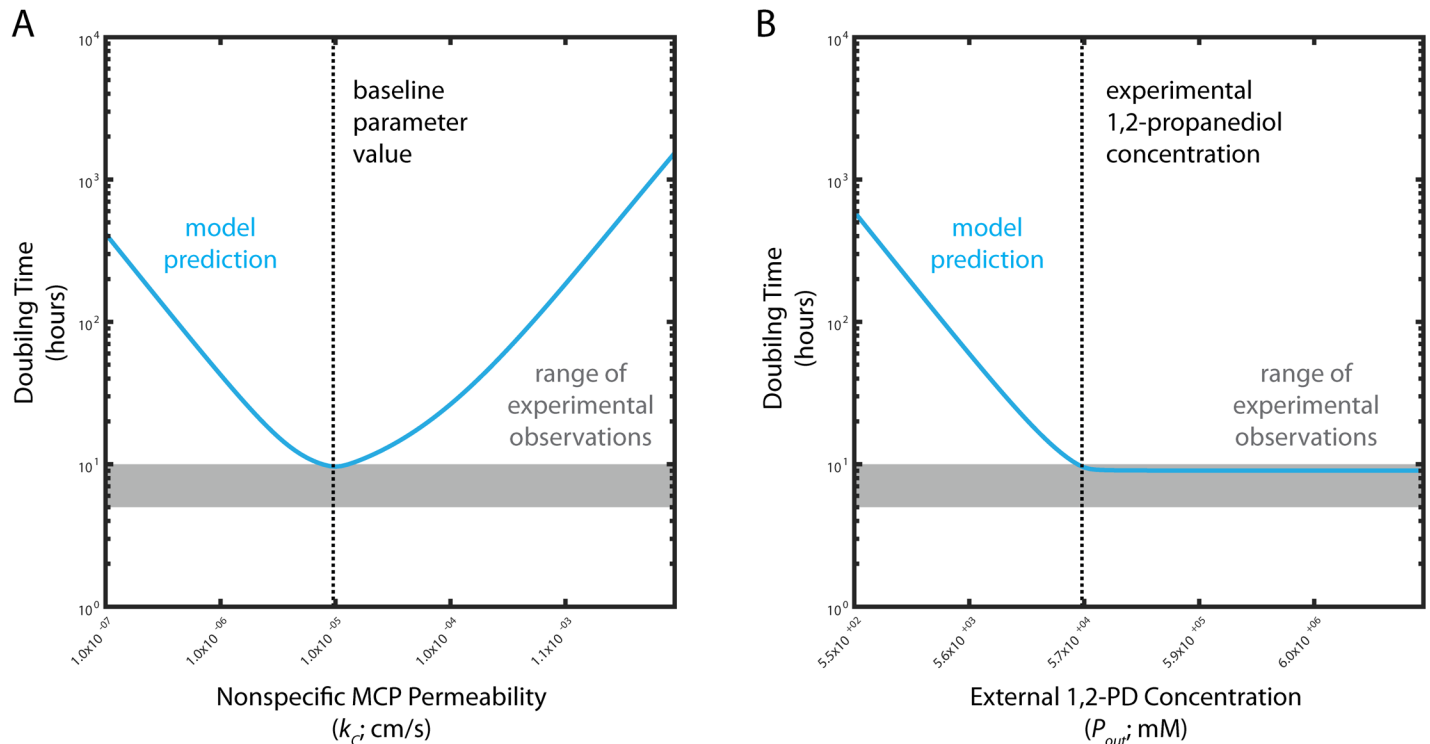
Fig 3. Predicted *S. enterica* doubling times for cells with MCPs as a function of (A) nonspecific MCP permeability k_c and (B) external 1,2-PD concentration P_{out}. Model predictions are shown in blue; observed doubling times for experiment are shown by the grey shaded area. The baseline k_c value and the typical experimental external 1,2-PD concentration are shown by black dashed lines in (A) and (B), respectively.

to treat fluxes in the model as at pseudo steady state, representing a single time point in a growth experiment. This accounts for the good congruence between our model results and the experimental measurements of steady-state *Salmonella* growth rates on 1,2-PD.

Another putative MCP function is the prevention of aldehyde loss into the growth medium. We quantify this phenomenon in our model as the net flux of propionaldehyde across the cell membrane into the extracellular space (so-called "propionaldehyde leakage"). This leakage is lower with MCPs than without ($3.52x10^{-13}$ μmol/cell-s as compared to $7.32x10^{-13}$ μmol/cell-s), but is the same order of magnitude as the flux through PduP/Q in both cases when the external 1,2-PD concentration is 55 mM (Fig 2D). For the case with MCPs, the flux through PduP/Q is approximately the same as the leakage flux, while leakage is over twice the PduP/Q flux in the

Table 2. Characteristic times for important processes in our model.

Process	Representation	Characteristic time (s)
Diffusion in the cell	$\tau_{cell}^{diff} = \frac{R_b^2}{D}$	$2.5x10^{-4}$
Diffusion in the Pdu MCP	$\tau_{MCP}^{diff} = \frac{R_c^2}{D}$	$1x10^{-5}$
Passive transport across the cell membrane	$\tau_{cell}^{trans} = \frac{R_b}{3k_m}$	$4x10^{-1}$
Passive transport across the MCP membrane	$\tau_{MCP}^{trans} = \frac{R_c}{3k_c}$	$3x10^{-1}$
PduCDE activity	$\tau_{CDE} = \frac{K_{MCDE}}{V_{CDE}}$	$3x10^{-3}$
PduP/Q activity	$\tau_{PQ} = \frac{K_{MPQ}}{2V_{PQ}}$	$3x10^{-1}$
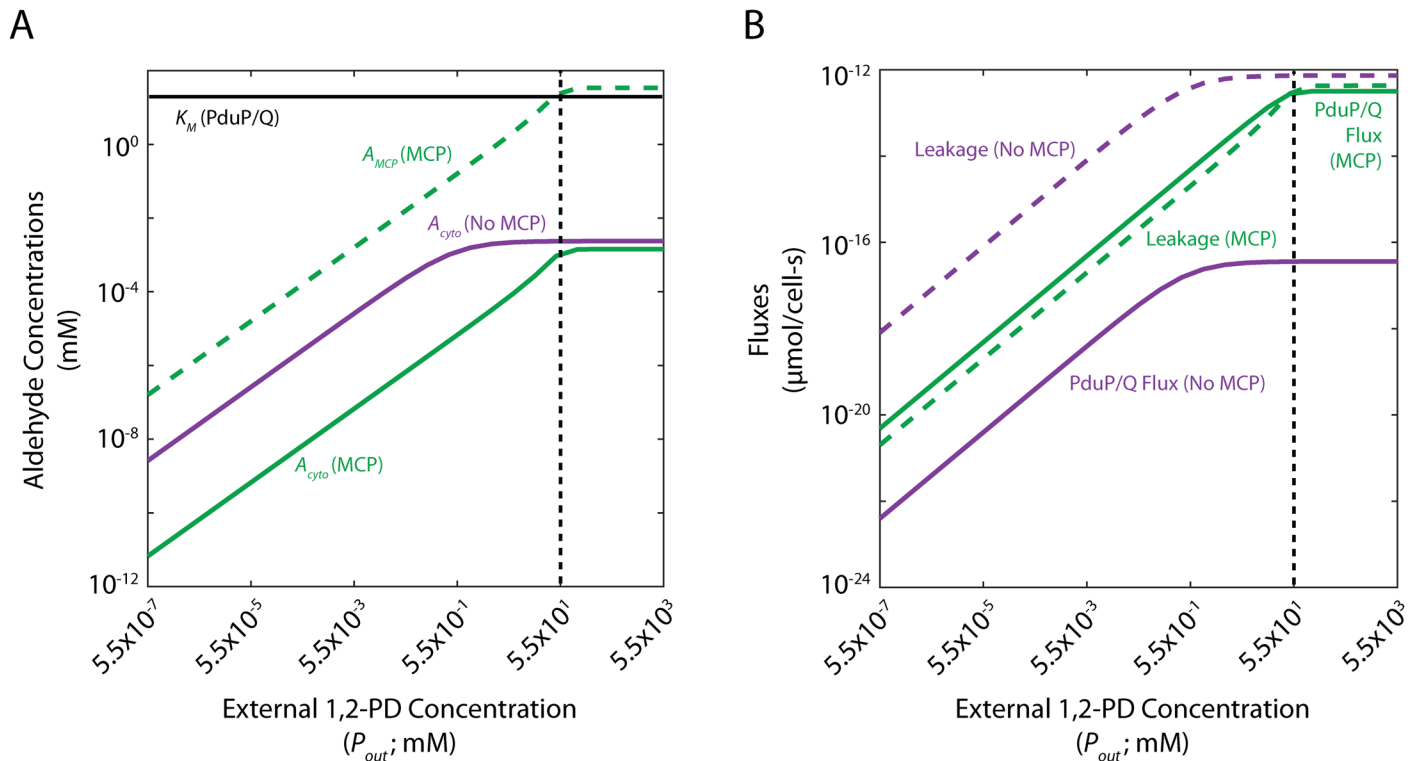
Fig 4. (A) Cytosolic propionaldehyde concentrations (A_{cyto}) with and without MCPs and MCP propionaldehyde concentrations (A_{MCP}) with MCPs and (B) steady-state fluxes through PduP/Q and propionaldehyde leakage across the cell membrane with and without MCPs. The baseline external 1,2-PD concentration is shown with a black dashed line; the K_M of PduP/Q is shown in (A) with a black solid line.

no-MCP case. The flux through PduP/Q, the leakage flux, and the concentrations of propional-dehyde in the cytosol and the MCP, are plotted for a range of external 1,2-PD concentrations in Fig 4. Fig 4A shows the absolute metabolite concentrations in the MCP (dashed) and cytosol (solid) in cells with (green) and without (purple) MCPs and Fig 4B shows the absolute aldehyde leakage (dashed) and PduP/Q flux (solid) for these two cases.

At high external 1,2-PD concentrations, the cytosolic propionaldehyde concentration is comparable with and without MCPs (Fig 4A). However, the kinetically relevant propionalde-hyde concentration in the vicinity of the PduP/Q enzymes is much higher in the MCP when MCPs than in the cytosol without MCPs. The flux through the PduP/Q enzymes is therefore much higher and the MCP functions primarily for flux enhancement. At low external 1,2-PD concentrations, the cytosolic propionaldehyde concentration is lower with MCPs, resulting in reduced aldehyde leakage into the extracellular space. Conversely, the kinetically relevant pro-pionaldehyde concentrations in the vicinity of the PduP/Q enzymes are more similar with and without MCPs in the case of low external 1,2-PD (and very low in either case), resulting in sim-ilar flux through the PduP/Q enzymes (Fig 4B). In the case of low external 1,2-PD concentra-tion, therefore, the relative difference in propionaldehyde leakage into the extracellular space is large, and the MCP functions primarily to reduce aldehyde leakage. It should be noted that localization to the MCP improves PduP/Q flux by at least 2 orders of magnitude at all external 1,2-PD concentrations, even though the flux for both strategies increases with external 1,2-PD.

There exists a transition from primarily flux enhancement to primarily aldehyde loss pre-vention as the external 1,2-PD concentration decreases. At high external 1,2-PD concentra-tions, cells with and without MCPs lose similar fluxes of propionaldehyde to the extracellular

space, but cells with MCPs experience much greater flux through PduP/Q; this is due to saturation of the PduP/Q enzymes by the high propionaldehyde concentration inside MCPs. At low external 1,2-PD concentrations, on the other hand, cells with MCPs are more parsimonious with respect to propionaldehyde, but gain a smaller benefit in flux through PduP/Q since the PduP/Q enzymes are not saturated, even with MCPs (S6 Fig).

Passive mechanisms are sufficient to support enzyme saturation at high external 1,2-PD concentrations, but active transport is necessary at low external 1,2-PD concentrations

We next determined the range of external 1,2-PD concentrations that saturate the PduP/Q enzymes in the MCP system. We explored this question using phase space representations of the saturation of the PduCDE and PduP/Q enzymes (Fig 5). In each phase space plot, two model parameters are varied and the effect on enzyme saturation is shown. We illustrate regions of parameter space in which neither enzyme is saturated (grey), only PduCDE is saturated (orange), or both enzymes are saturated (blue). Saturation of PduP/Q without saturation of PduCDE was not observed. Also shown in each phase space are isolines illustrating the parameter values for which the cytosolic concentration of propionaldehyde is 10 nM (0.001% of the toxicity limit) and 1 uM (0.1% of the toxicity limit), as well as dotted lines indicating the baseline parameter estimates used in the model (Table 1). Recall that the toxicity limit for intracellular propionaldehyde is approximately 8 mM. Phase space representations of this kind are useful because they allow examination of the behavior of the system over a very wide range of parameter space, encompassing the entire range of physically reasonable values for each parameter in question.
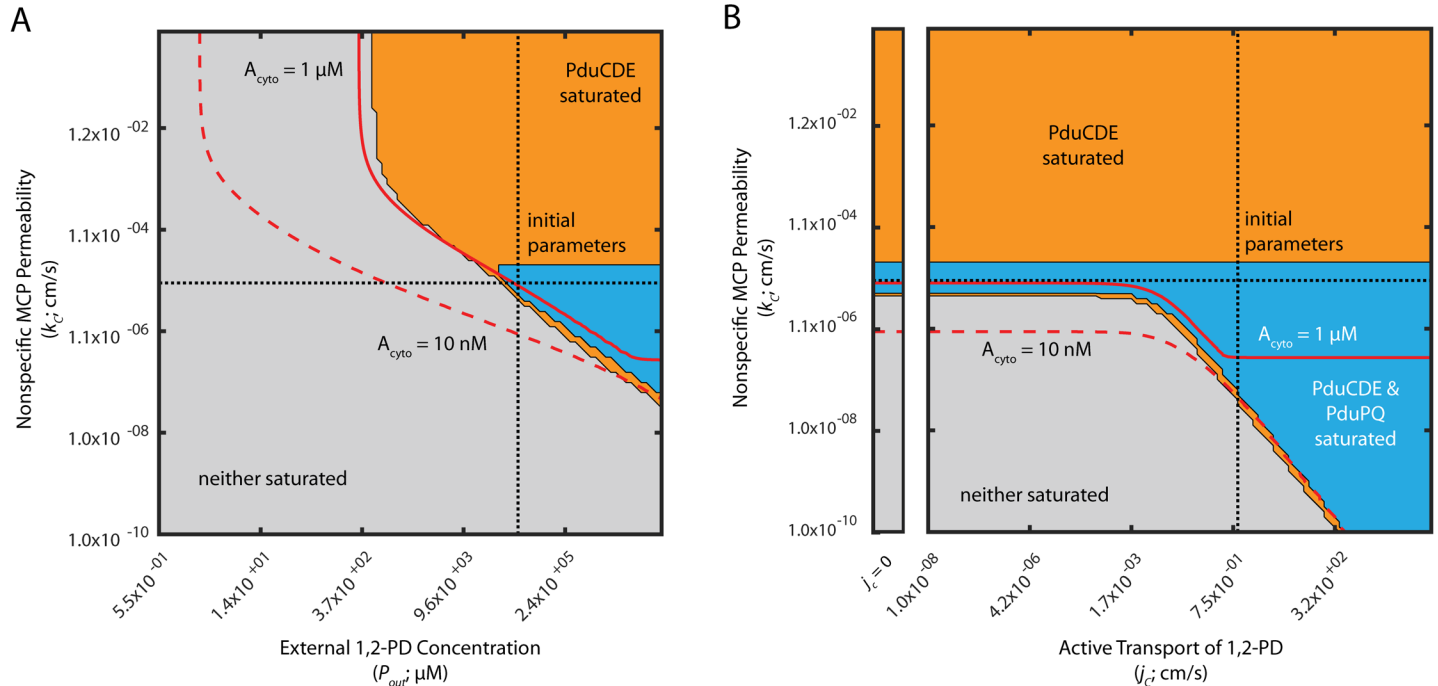
Fig 5. Saturation phase spaces of PduCDE and PduP/Q (A) with respect to P_{out} and k_c, and (B) with respect to j_c and k_c. Regions of saturation (concentration of substrate > K_M of the appropriate enzyme) are plotted in blue when PduCDE and PduP/Q are saturated, orange when only PduCDE is saturated, and in grey when neither enzyme is saturated. Red solid lines indicate when A_{cyto} is 1 μM; red dashed lines indicate when A_{cyto} is 10 nM. Black finely dashed lines indicate the baseline parameter values used in the model of the Pdu MCP. The inset to the left in (B) reflects the behavior when $j_c = 0$.

https://doi.org/10.1371/journal.pcbi.1005525.g005

In [Fig 5A], for instance, the saturation of PduCDE and PduP/Q is examined as a function of the value of the nonspecific MCP membrane permeability k_c and the external 1,2-PD concentration P_{out}. The blue region indicating saturation of both PduCDE and PduP/Q occurs only at high P_{out} values comparable to or higher than the baseline concentration. PduCDE alone can be saturated for a wider range of P_{out}, as indicated by the extent of the orange region. Interestingly, for a broad range of P_{out} concentrations, neither enzyme can be saturated no matter the value of the nonspecific MCP permeability k_c. We therefore conclude that PduCDE and PduP/Q can be saturated by adjusting k_c for a P_{out} greater than 50 mM, but for lower P_{out} concentrations no value of k_c achieves enzyme saturation. We expect that these lower concentrations are relevant for MCP-mediated metabolism *in vivo* because we observe that a P_{Pdu}::*gfp* reporter is activated for 1,2-PD concentrations as low as 55 μM [24].

Extending this analysis to the other passive diffusion mechanisms considered in the model, we find that PduP/Q can also be saturated for a range of external 1,2-PD concentrations by modulating the cell membrane permeability to 1,2-PD, k_m^P, and the cell membrane permeability to propionaldehyde, k_m^A; but that for each parameter there exists a lower limit of external 1,2-PD concentration (30 mM and 20 mM, respectively) below which PduP/Q cannot be saturated by passive mechanisms ([S7A and S7B Fig]).

The *pduF* ORF of the *S. enterica* Pdu operon is a putative membrane protein, and is speculated to encode a 1,2-PD transporter [25]. We therefore explored the possible role of active 1,2-PD transport across the cell membrane in the saturation of the PduP/Q enzymes. Figs [5] and [S7] shows phase space representations of PduCDE and PduP/Q saturation with respect to active 1,2-PD transport and two passive transport parameters when the external 1,2-PD concentration is 55 mM; [S8 Fig] shows the same analyses when the external 1,2-PD concentration is 0.5 mM. We find that active transport of 1,2-PD is dispensable at high external 1,2-PD concentrations (*i.e.* 55 mM), but not at lower external 1,2-PD concentrations (*i.e.* 0.5 mM). When the external 1,2-PD concentration is 55 mM, the nonspecific MCP membrane permeability, k_c, can adopt a value such that both PduCDE and PduP/Q are saturated for any value of the velocity of active 1,2-PD transport across the cell membrane, j_c ([Fig 5A]). The same is true of the cell membrane permeability to 1,2-PD, k_m^P, when the external 1,2-PD concentration is 55 mM ([S7C Fig]). In contrast, when the external 1,2-PD concentration is 0.5 mM, there exists a minimum value (1 cm/s) of the velocity of active 1,2-PD transport across the cell membrane, j_c, below which PduP/Q cannot be saturated solely by modulating the MCP shell passive diffusion parameter k_c ([S8A Fig]). Similar minima exist at active transport velocities of $2x10^{-5}$ cm/s and 0.3 cm/s for the cell membrane passive diffusion parameters k_m^A and k_m^P ([S8B and S8C Fig]). At this lower external concentration of 1,2-PD, therefore, active transport of 1,2-PD across the cell membrane may play an important role. Indeed, with high rates of active transport of $6x10^3$ cm/s, PduP/Q can be saturated for an extremely wide range of external 1,2-PD concentrations ([S9 Fig]).

We can further understand these trends by examining the analytical solution to the model. The relative contribution of active transport to 1,2-PD transport across the cell membrane (as compared to passive diffusion) is expressed by the quantity $\lambda = 1 + \frac{j_c}{k_m^P}$. This suggests that active transport can only be significant if $\frac{j_c}{k_m^P} > 1$. Furthermore, transport of 1,2-PD across the cell membrane only impacts the steady-state 1,2-PD concentration in the MCP when $\lambda p^* \approx \Gamma_{CDE}$, where $\lambda p^* = \left(1 + \frac{j_c}{k_m^P}\right)\frac{P_{out}}{K_{MCDE}}$ represents active and passive transport across the cell membrane and $\Gamma_{CDE} = \frac{\tau_{MCP}^{diff}}{\tau_{CDE}}\left(\frac{\tau_{cell}^{trans}}{\tau_{cell}^{diff}} + \frac{\tau_{MCP}^{trans}}{\tau_{MCP}^{diff}} + \frac{1}{3}\rho + \frac{1}{3}\right)$ represents the balance between transport and reaction processes. From the analytical solution in [S1 Text], active transport only bears on

the solution when $\frac{j_c}{k_m^P} > 1$ and $\lambda p^* \approx \Gamma_{CDE}$. In S7, S8 and S9 Figs, when the external 1,2-PD concentration is high, λp^* is large relative to Γ_{CDE} and changes in λ are inconsequential except at large λ values (when k_m^P is small). When the external 1,2-PD concentration is low, however, as in S4 Fig, $\lambda p^* \approx \Gamma_{CDE}E$ and active transport is therefore consequential for a large range of k_m^P. We also observe that active transport only impacts saturation when $\frac{j_c}{k_m^P} > 1$, as expected from the analytical solution.

## Selective MCP permeability is not absolutely required to saturate PduP/Q

Experimental results suggest that the protein membrane surrounding the Pdu MCP might exhibit selective permeability [26]. We therefore explored under what conditions such selective permeability was advantageous for MCP function. We first consider the simple case of nonspecific permeability.

We find that an optimal non-selective MCP shell permeability exists with respect to the kinetically relevant propionaldehyde concentration in the vicinity of the PduP/Q enzymes (Fig 6A). This optimum value (10^{-5} cm/s) of a single nonspecific permeability k_c reflects a tradeoff between 1,2-PD entry to the MCP and trapping of propionaldehyde within the MCP. The non-selective permeability must be high enough for adequate entry of the PduCDE substrate 1,2-PD, but low enough to contribute to the accumulation of the PduP/Q substrate propionaldehyde within the organelle. This can be seen clearly when the permeabilities of the MCP membrane to 1,2-PD and propionaldehyde are varied separately (Fig 6B and 6C). Lower permeability to propionaldehyde is unambiguously advantageous for trapping propionaldehyde in the MCP. Higher permeability to 1,2-PD, k_c^P, also increases propionaldehyde concentration inside the MCP, until the permeability is sufficient to equalize the cytosolic and MCP 1,2-PD concentrations, at which point there is no further improvement.

The presence of an optimal permeability persists when the ratio of k_c^P to k_c^A is fixed at 0.1 or 10 and the values are varied together, maintaining this ratio (S10 Fig). Moreover, decreasing k_c entails a tradeoff between leakage prevention and flux enhancement, the two aspects of Pdu MCP function (S11 Fig). At low k_c (less than 10^{-7} cm/s), aldehyde leakage is prevented, but flux is low; near the optimal k_c for flux enhancement (10^{-5} cm/s), leakage is comparable with and without MCPs. At high k_c (greater than 1), the system approaches the case of scaffolding, with only a small flux enhancement and no leakage prevention.

We determine the potential benefit of selective permeability by examining the enzyme saturation phase space with respect to the specific permeabilities k_c^A and k_c^P (Fig 6D). The $k_c^A = k_c^P$ line, along the diagonal, in this subspace indicates the performance of the system when the MCP permeability is non-selective. This line passes through the blue region in which PduP/Q is saturated, indicating that selective permeability is not absolutely required for efficient performance. However, selective permeability permits a broader range of k_c^A and k_c^P values to saturate PduP/Q (Fig 6D). It is interesting to note that MCP permeability to propionaldehyde must be lower than or equal to MCP permeability to 1,2-PD. As observed above, decreasing MCP permeability to propionaldehyde is unambiguously beneficial for flux, while decreasing the MCP permeability to 1,2-PD below the MCP permeability to propionaldehyde is detrimental to relative flux (S11 Fig). It is also important to note, however, that increasing the concentration of propionaldehyde inside the MCP beyond the concentration required to saturate PduP/Q is not beneficial, since there is no increase in flux, but propionaldehyde leakage increases.
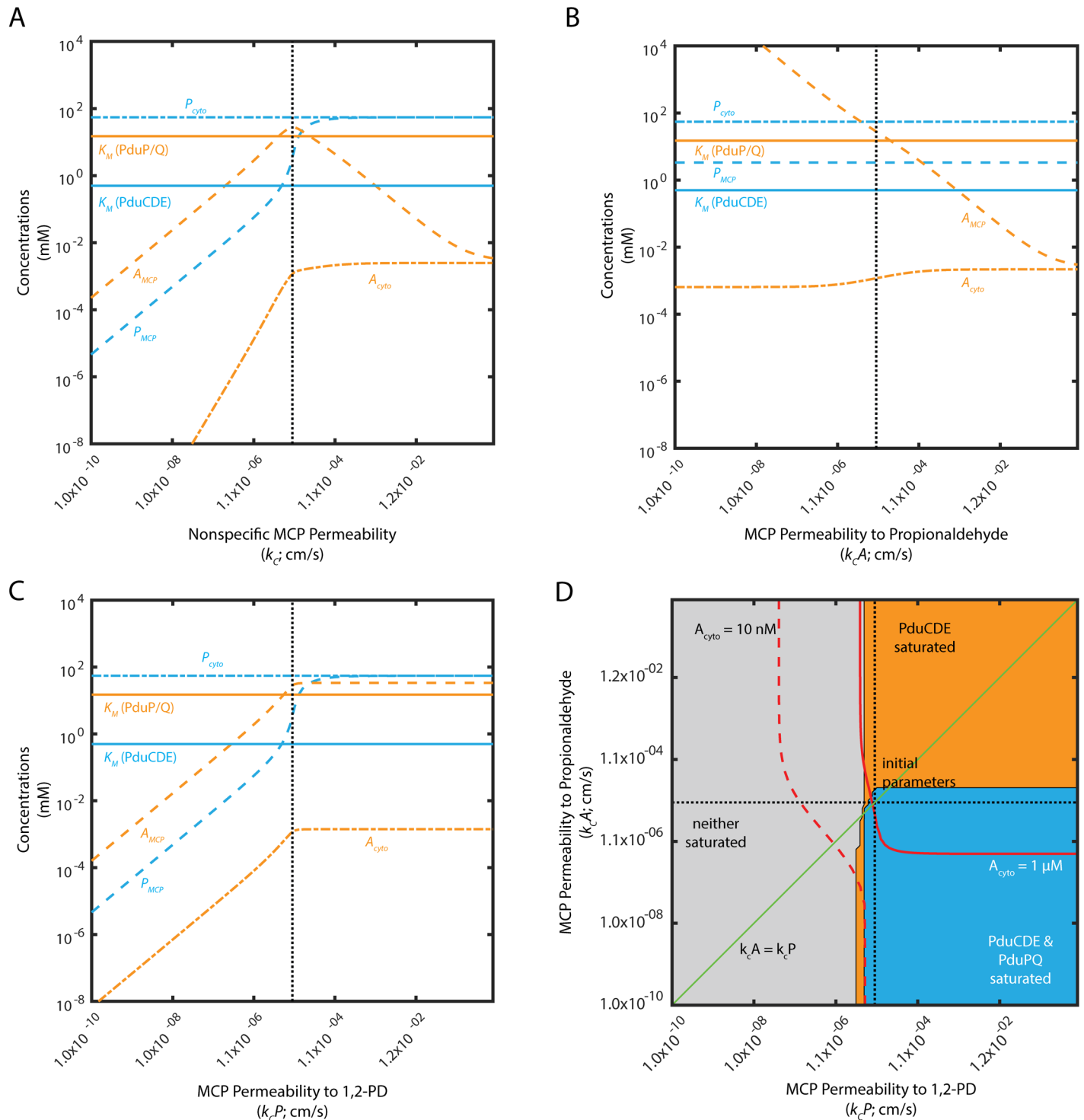
Fig 6. Mean concentrations of 1,2-PD and propionaldehyde in the MCP (P_{MCP}; A_{MCP}) and cytosol (P_{cyto}; A_{cyto}) as a function of (A) k_c when $k_c = k_c^A = k_c^P$; (B) k_c^A when $k_c^P = 10^{-5}$ cm/s; and (C) k_c^P when $k_c^A = 10^{-5}$ cm/s. Saturation phase space of PduCDE and PduP/Q with respect to (D) k_c^A and k_c^P. In (A), (B), and (C), K_M of PduCDE and PduP/Q are shown as solid lines. The baseline permeabilities are shown with a black dashed line. In (D), regions of saturation (concentration of substrate > K_M of the appropriate enzyme) are plotted in blue when PduCDE and PduP/Q are saturated, orange when only PduCDE is saturated, and in grey when neither enzyme is saturated. Red solid lines indicate when A_{cyto} is 1 μM; red dashed lines indicate when A_{cyto} is 10 nM. Black dashed lines indicate the baseline parameter values used in the model of the Pdu MCP. Green line indicates $k_c^A = k_c^P$.

Discussion

By analyzing the closed-form analytical solution to our mechanistic model of Pdu MCP function, we first find that flux enhancement may play a more significant role in MCP function than previously thought. Secondly, our results suggest that active transport of 1,2-PD across the cell membrane may in many cases contribute significantly to MCP function. Lastly, we find that, while not always required for MCP function, selective MCP membrane permeability can enhance MCP function.

Flux enhancement is a key facet of MCP function

Experimental investigations of Pdu MCP function have consistently demonstrated two key phenotypes for strains that express the Pdu enzymes but fail to form MCPs: a slower growth rate and increased propionaldehyde concentration in the media [21]. Slower growth could be attributable to two phenomena: "passive" growth retardation due to lower carbon flux through the Pdu metabolon, and "active" growth retardation due to the toxic effects of propionaldehyde in the cytosol. This second form of growth defect is linked to the accompanying observation that strains lacking MCPs have an increased rate of propionaldehyde leakage into the extracellular space. These two forms of growth retardation cannot be distinguished by an *in vivo* experiment measuring the growth of cells and the bulk concentrations of the various metabolites. Our simple model supports the idea that both of these phenotypes contribute to changes in growth rate: we observe that cells with MCPs have both higher flux through PduP/Q and lower cytosolic concentrations of propionaldehyde than cells without MCPs, and that cells with MCPs exhibit lower aldehyde flux into the growth medium than cells without MCPs. Additionally, experiments indicate similar 1,2-PD depletion from the growth medium with and without MCPs, a phenotype that is evident in the comparable PduCDE fluxes predicted by our model with and without MCPs [21]. Together these observations indicate that our model captures the important principles of Pdu MCP function. Indeed, we propose that while toxicity reduction likely plays a role in MCP function, flux enhancement is a crucial, and underappreciated, consequence of encapsulation. This in turn suggests that experiments should explore the relative contributions of flux enhancement and toxicity mitigation in more detail. For instance, the effects of propionaldehyde toxicity could be characterized by determining the degree to which aldehyde leakage from MCP-defective cells leads to increased formation of covalent adducts to the cellular genome and proteome.

Pdu MCPs as compared to other organization strategies

Other enzyme organization strategies, notably enzyme scaffolds based on DNA, RNA, and protein [26–28], have been shown to increase the flux through enzymatic pathways, and membrane-less organelles and enzyme clusters are also thought to confer kinetic enhancement [29–31]. While colocalization can generally be expected to enhance flux in many cases, the extent of the enhancement will depend on the kinetics of the enzymes in question and the other cellular processes involved, such as the loss or toxicity of an intermediate. Indeed, for the Pdu MCP system, we predict only a modest benefit from scaffolding as compared to the benefit derived from encapsulation. The problem of organization choice awaits a comprehensive analysis of the relative benefits of scaffolding and other strategies for diverse enzyme systems.

Other compartment-based strategies such as the carboxysome also function to increase flux through the enclosed pathway [22, 32]. Compartment-based organization differs from the above systems in that it imposes a diffusive barrier that allows the partitioning of intermediates to a subcellular compartment. The balance between substrate entry and intermediate trapping therefore results in an optimum nonspecific permeability of the diffusive barrier in the

carboxysome case. Notably, we find that such an optimum exists in the Pdu MCP case, as well. The kinetics of the cascade in the Pdu MCP, however, are fundamentally different from that of the carboxysome, since the first step of the cascade, catalyzed by PduCDE, is irreversible. This leads to an increasing benefit of selective permeability, accrued due to the accumulation of intermediates, that exceeds what is predicted for the carboxysome [32].

It is notable that depsite these key differences, we predict a similar overall kinetic enhancement effect for the Pdu MCP system, as compared to these other organization strategies. This suggests that nature has evolved disparate enzyme organization modes with convergent overall benefits, providing the metabolic engineer with a wide range of potential organizational options for a given heterologous pathway.

MCP function depends on extrinsic factors

Many behaviors in our model depend strongly on external 1,2-PD concentration. Therefore, care must be taken in applying results from experiments conducted at high 1,2-PD concentrations (55 mM) in the laboratory to Pdu MCP function inside the host, and in interpreting the results of batch-wise culture experiments in which the external 1,2-PD concentration changes during the experiment, decreasing from 55 mM to 1 mM [21]. We find that MCP function, as quantified by the relative PduP/Q flux and the relative propionaldehyde flux into the extracellular space, changes in response to factors extrinsic to the cell, such as external 1,2-PD concentration. Indeed, these may change during a single experiment: for example, cells without MCPs may be observed to leak slightly more propionaldehyde into the growth medium than cells with MCPs when grown at high external 1,2-PD concentrations, but this leakage discrepancy may increase over the course of a batch experiment during which 1,2-PD is depleted from the growth medium. Whether or not PduP/Q can be saturated without active transport also depends on external 1,2-PD concentration; our model suggests that active transport of 1,2-PD across the cell membrane is dispensable at high external 1,2-PD concentrations, but not as the external 1,2-PD concentration decreases. These mechanistic observations suggest that experiments to determine the function of the *pduF* gene product, for instance, should be undertaken in low 1,2-PD concentration so that active transport is made relevant to growth.

It is unknown what external concentration of propionaldehyde is encountered in the host gut by invading *Salmonella*, but the concentration is likely to be low due to the toxicity of aldehyde species to eukarya. Gnotobiotic mice bearing only *B. thetaiotaomicron* develop 10-50 μM of 1,2-PD in the gut [33], but neither the concentrations in the presence of the full microbiota nor the associated concentrations of propionaldehyde are known. With respect to laboratory growth experiments, the propionaldehyde concentration in the growth medium is observed to increase in batch-wise growth experiments, up to concentrations around 10 mM [21]. The calculations above were performed assuming no external propionaldehyde, but we tested our model at a range of external propionaldehyde concentrations (1 μM, 1 mM, and 10 mM; S12 Fig) and found that the qualitative behavior of the system did not change with increasing external propionaldehyde concentration. The regions of parameter space in which PduP/Q could be saturated were broader at higher propionaldehyde concentrations, but at the cost of high cytosolic aldehyde concentrations equilibrated with the external concentration.

Selective MCP membrane permeability is not required, but is often advantageous

Recent evidence suggests that the Pdu MCP shell may be selectively permeable to propionaldehyde as compared to other metabolites [34]. Our model suggests that, while the saturation of PduP/Q enzymes can be achieved without selective permeability in particular cases, it is true

in general that selective permeability can enhance Pdu MCP function. In contrast, selective permeability of the MCP shell does not improve the function of a related system, the CO_2 concentrating mechanism [32]. The monotonic benefit of selective permeability in the Pdu system is due to PduCDE catalyzing an essentially irreversible reaction, whereas the enzyme playing the equivalent role in the CO_2 concentrating mechanism is reversible. Trapping of propionaldehyde in the MCP by decreasing the relative permeability of the MCP shell to propionaldehyde can therefore saturate the PduP/Q enzymes if the permeability of the MCP to 1,2-PD is sufficiently high. Similarly, if the permeability of the MCP to propionaldehyde is sufficiently low, the permeability to 1,2-PD can be increased to saturate PduP/Q. This putative trapping mechanism is in congruence with the *in vitro* observation that small molecule efflux from a protein nanoreactor can be affected by the chemical character of the reactor pores [35]. Studies of substrate channeling in enzyme scaffolds also emphasize the importance of creating a high substrate concentration in the vicinity of downstream enzymes [28, 36]. In the case of a microcompartment, the shell diffusion barrier creates a concentration differential across the MCP shell, rather than a very high local concentration of enzymes enforcing a local diffusion gradient.

One must be careful in the interpreting our results for the limits of extreme selectivity (that is $k_c^A << k_c^P$). In the absence of energetic input, there must be a physiological limit on how low the MCP permeability to propionaldehyde can be relative to 1,2-PD. In addition, the reaction catalyzed by PduCDE will not remain irreversible under extremely high concentrations of propionaldehyde. Without these limits, the cell could create a Maxwell's demon by concentrating infinite amounts of propionaldehyde. Even in less extreme cases, we still predict a significant flux enhancement. Interestingly, our results suggest that selective permeability, while often advantageous, is by no means required for significant flux enhancement (Fig 2).

Further experimental determination of the MCP shell permeability is required to determine in what parameter regime the Pdu MCP system operates, and whether selectivity is required *in vivo*. Our model predicts an optimal nonspecific Pdu MCP permeability of 10^{-5} cm/s, we can compare this value to future experimental data for the various relevant metabolites. The permeability we predict is much lower than would be estimated based on free diffusion through an area equivalent to the cumulative area of the pores in the MCP shell (on the order of $1 - 10$ cm/s). The phenomenon of surprisingly low apparent permeability of a protein shell has been predicted previously [35], and is likely rooted in the fact that the Debye length, governing the distance at which electronic interactions occur between the amino acid residues lining the pore and the client small molecules, extends across the entire pore area. Excluded-volume models of apparent diffusivity in the pore, therefore, do not apply. Below we discuss possible future approaches to understanding this phenomenon.

Implications for engineering encapsulation of heterologous pathways

Our results have important implications for microbiological studies of MCP function and for the application of encapsulation to synthetic biology. Interestingly, our model indicates that the encapsulation of enzymes in a subcellular compartment can dramatically improve flux through the encapsulated pathway, in addition to reducing the concentrations of intermediates in the cytosol, simply by imposing a non-specific diffusion barrier. This reinforces the notion that encapsulation is a promising strategy to improve the yield and titer of heterologous enzymatic pathways that fail to function in a cytosolic context.

Our results suggest that a heterologous pathway must possess several key characteristics in order to benefit from encapsulation. First, the substrate of the pathway must be capable of entering the MCP lumen through the MCP shell pores sufficiently quickly to support the first

pathway reaction. Without this property, the pathway cannot function efficiently in the MCP context. Secondly, the escape of the intermediate species must be sufficiently retarded as to allow the accumulation of significant concentration gradients across the MCP shell. Our model indicates that this phenomenon is at the heart of MCP-dependent flux enhancement. Finally, the second enzyme (of a two-enzyme pathway) should be relatively slow (*i.e.* in terms of $\frac{k_{cat}}{K_M}$) so that the accumulation of intermediates in the MCP results in a substantial increase in the enzymatic rate. All of these characteristics are true of the native Pdu pathway, and we predict that heterologous pathways sharing these characteristics will likewise enjoy a flux increase upon encapsulation. These conclusions stem from the general topology of the phase spaces we analyzed, and are likely to be qualitatively similar across diverse biochemical pathways. Additionally, active transport of the substrate of the first enzyme, and selective microcompartment permeability with respect to the various species in question, may be advantageous but not necessary for productive encapsulation.

Further investigation is required to quantitatively inform the selection of appropriate pathways for encapsulation, since the system's behavior may vary somewhat with the biophysical properties of the species involved in the pathway. The framework presented here is amenable to analyzing the performance of many such candidate pathways. We also find that, for the Pdu system, encapsulation is superior to scaffolding in enhancing pathway flux, and future efforts will explore what characteristics render certain pathways amenable to encapsulation versus scaffolding and other organization strategies.

Engineering efforts have recently demonstrated control of the heterologous enzymatic contents of the Pdu MCP [24]. We therefore considered the effect of increasing or decreasing the enzymatic concentration inside the Pdu MCP on the behavior of the model. In Fig 5 we illustrate the effects of MCP permeability, external 1,2-PD concentration, and active 1,2-PD transport on the saturation of PduCDE and PduP/Q. We recapitulate these phase spaces in S13 Fig for $N_{total} = N_{PQ} + N_{CDE}$ 100-fold higher and 100-fold lower than observed in wild type Pdu MCPs [12]. We observe that the topology of the phase spaces remains the same (with a concomitant shift in the optimal nonspecific MCP permeability), indicating that our analysis as to the qualitative characteristics of the Pdu MCP system will extend to higher and lower enzyme loadings.

Outstanding questions for modeling and experiment

Many questions also remain to be addressed both computationally and experimentally with respect to native MCP function. First, in our model we neglect $NAD^+/NADH$ cofactor recycling at steady state by setting the rate of PduP catalysis equal to that of PduQ. Future models could incorporate cofactor-dependent kinetics of PduP/Q, in addition to including the effect of B_{12} recycling within the MCP shell on the kinetics of PduCDE. Further kinetic studies of the relevant enzymes will be required to inform such models. Also lacking at this time are detailed simulations of the structure and dynamics of the Pdu shell pores, particularly with respect to the diffusion of species of varying size and charge. High resolution modeling, such as molecular dynamics simulations of the pore, could aid in determining how low permeabilities as low as 10^{-5} cm/s could be achieved. Studies of this kind would be complemented by direct experimental measurements of the permeability of the MCP shell to various species. These studies would also inform the selection of heterolgous pathways with appropriate diffusion characteristics. Our model makes quantitative predictions for the permeabilities of small molecule metabolites such as 1,2-PD and propionaldehyde, and also for the permeability of the MCP shell to cofactors like $NAD^+/NADH$ (insomuch as we assume that the MCP shell is impermeable to these species), all of which can be compared to experimental results.

Also of interest are experimental investigations as to the possibility of active 1,2-PD transport across the cell membrane. Our results suggest that such active transport would be advantageous at low external 1,2-PD concentrations but dispensable at high external 1,2-PD concentrations, complicating experiments. The putative membrane-bound Pdu gene product *pduF* is of primary interest in this regard. Lastly, experimental observations of the absolute 1,2-PD and propionaldehyde concentrations encountered by invading *Salmonella* in the host gut and in the environment at large will be valuable in constraining future modeling efforts to pathogenically relevant metabolite concentrations, and in comparing the conditions faced by free-living and host-associated pathogens. Existing measurements of 10-50 μM 1,2-PD were made in germ-free or gnotobiotic conditions [33], and may differ in the presence of the normal microbiota.

Supporting information

S1 Text. Mathematical appendix. This appendix elaborates on the model formulations in the Models section and on the equations used in the analytical and numerical code to generate the plots and other figures.
(PDF)

S1 Fig. Comparison of analytical solution assuming constant concentrations in the MCP (solid lines) and numerical solutions from the edge (circles) and center (triangles) of the MCP for 1,2-PD (blue) and propionaldehyde (orange). The baseline parameter values are shown with a black dashed line. The K_M of the PduCDE and PduP/Q enzymes are plotted in blue and orange lines, respectively.
(TIF)

S2 Fig. Sensitivity analysis of total pathway flux with respect to model parameters. Plotted is the relative flux after the perturbation as compared to the flux using the initial parameters. MCP organization is shown in (A), (B), (C), and (D); scaffold organization is shown in (E), (F), (G), and (H). (A), (C), (E), and (G): P_{out} = 55 mM. (B), (D), (F), and (H): P_{out} = 0.5 mM. (A), (B), (E), and (F): no active transport of 1,2-PD. (C), (D), (G), and (H): j_c = 1 cm/s. Orange bars indicate the change in flux upon a 10% decrease in the indicated parameter; blue bars indicate the change in flux upon a 10% increase in the indicated parameter. Grey box indicates a 10% change in the relative flux. Red dashed line indicates the flux based on the initial parameters.
(TIF)

S3 Fig. Predicted *S. enterica* doubling times for cells with MCPs as a function of (A) total number of PduCDE and PduP/Q enzymes N_{total} and (B) fraction of total enzymes that are PduP/Q $\frac{N_{PQ}}{N_{total}}$. Model predictions are shown in blue; observed doubling times for experiment are shown by the grey shaded area. The experimentally observed N_{total} and $\frac{N_{PQ}}{N_{total}}$ values are shown by black dashed lines in (A) and (B), respectively. $\frac{N_{PQ}}{N_{total}}$ is held constant in (A) and N_{total} is held constant in (B).
(TIF)

S4 Fig. Concentration profiles as a function of r for a cell with (A) no MCPs; (B) a scaffold with no diffusion limitation (k_c = 10^3); (C) MCPs (k_c = 10^{-5}); and (D) sparingly permeable MCPs (k_c = 10^{-7}). 1,2-PD in the MCP (P_{MCP}) and in the cytosol (P_{cyto}) are plotted in blue and propionaldehyde in the MCP (A_{MCP}) and in the cytosol (A_{cyto}) in orange. The K_M of the PduCDE and PduP/Q enzymes are plotted in blue and orange dashed lines, respectively.
(TIF)

S5 Fig. (A) Cytosolic aldehyde concentration (A_{cyto}) with and without MCPs and MCP aldehyde concentration (A_{MCP}) with MCPs; (B) relative carbon flux through PduP/Q ($\frac{flux_{MCP}}{flux_{NoMCP}}$) and relative aldehyde leakage rate ($\frac{leakage_{NoMCP}}{leakage_{MCP}}$); and (C) relative flux through the PduP/Q enzymes (with MCPs/without MCPs) and relative propionaldehyde leakage across the cell membrane (without MCPs/with MCPs) as a function of k_m^A. The baseline k_m^A value is shown with a black dashed line.
(TIF)

S6 Fig. Relative flux through the PduP/Q enzymes (with MCPs/without MCPs) and relative propionaldehyde leakage across the cell membrane (without MCPs/with MCPs) as a function of external 1,2-PD concentration. The baseline external 1,2-PD concentration is shown with a black dashed line.
(TIF)

S7 Fig. Saturation phase spaces of PduCDE and PduP/Q (A) with respect to P_{out} and k_m^P, (B) with respect to P_{out} and k_m^A, and (C) with respect to j_c and k_m^P when P_{out} is 55 mM. Regions of saturation (concentration of substrate $> K_M$ of the appropriate enzyme) are plotted in blue when PduCDE and PduP/Q are saturated, orange when only PduCDE is saturated, and in grey when neither enzyme is saturated. Red solid lines indicate when A_{cyto} is 1 μM; red dashed lines indicate when A_{cyto} is 10 nM. Black dashed lines indicate the baseline parameter values used in the model of the Pdu MCP.
(TIF)

S8 Fig. Saturation phase spaces of PduCDE and PduP/Q with respect to (A) j_c and k_c, (B) with respect to j_c and k_m^P, and (C) with respect to j_c and k_m^A when P_{out} is 0.5 mM. Regions of saturation (concentration of substrate $> K_M$ of the appropriate enzyme) are plotted in blue when both enzymes are saturate, orange when only PduCDE is saturated, and in grey when neither enzyme is saturated. Red solid lines indicate when A_{cyto} is 1 μM; red dashed lines indicate when A_{cyto} is 10 nM. Black dashed lines indicate the baseline parameter values used in the model of the Pdu MCP.
(TIF)

S9 Fig. Saturation phase spaces of PduCDE and PduP/Q with respect to (A) P_{out} and j_c, and (B) with respect to P_{out} and k_m^P. Regions of saturation (concentration of substrate $> K_M$ of the appropriate enzyme) are plotted in blue when both enzymes are saturate, orange when only PduCDE is saturated, and in grey when neither enzyme is saturated. Red solid lines indicate when A_{cyto} is 1 μM; red dashed lines indicate A_{cyto} is 10 nM. Black dashed lines indicate the baseline parameter values used in the model of the Pdu MCP.
(TIF)

S10 Fig. Mean concentrations of 1,2-PD and propionaldehyde in the MCP (P_{MCP}; A_{MCP}) and cytosol (P_{cyto}; A_{cyto}) as a function of (A) k_c^A when $k_c^P = \mathbf{0.1} x k_c^A$ and (B) k_c^A when $k_c^P = \mathbf{10} x k_c^P$. K_M of PduCDE and PduP/Q are shown as solid lines. The baseline permeabilities are shown with a black dashed line.
(TIF)

S11 Fig. (A,D,G) Cytosolic aldehyde concentration (A_{cyto}) with and without MCPs and MCP aldehyde concentration (A_{MCP}) with MCPs; (B,E,H) absolute flux through PduP/Q and aldehyde leakage from the cell with and without MCPs; and (C,F,I) relative carbon flux through PduP/Q ($flux_{MCP}/flux_{NoMCP}$) and relative aldehyde leakage rate

(*leakage$_{MCP}$/leakage$_{NoMCP}$*). As a function of (A,B,C) $k_c = k_c^A = k_c^P$; (D,E,F) k_c^A; and (G,H,I) k_c^P. The baseline permeabilities are shown with a black dashed line.
(TIF)

S12 Fig. (A, C, E) Saturation phase space of PduCDE and PduP/Q with respect to k_c^A and k_c^P and (B, D, F) saturation phase space of PduCDE and PduP/Q with respect to k_c^A and j_c for external propionaldehyde concentrations of (A, B) 1 μM, (C, D) 1 mM, and (E, F) 10 mM. Regions of saturation (concentration of substrate $> K_M$ of the appropriate enzyme) are plotted in blue when both enzymes are saturated, orange when only PduCDE is saturated, and in grey when neither enzyme is saturated. Red solid lines indicate when A_{cyto} is 1 μM; red dashed lines indicate when A_{cyto} is 10 nM. Black dashed lines indicate the baseline parameter values used in the model of the Pdu MCP. Green line in (A, C, E) indicates when $k_c^A = k_c^P$.
(TIF)

S13 Fig. Saturation phase space of PduCDE and PduP/Q with respect to k_c and P_{out} and with respect to k_c and j_c for total enzyme concentrations N_{total} 100-fold higher and lower than the baseline parameter value. Regions of saturation (concentration of substrate $> K_M$ of the appropriate enzyme) are plotted in blue when both enzymes are saturated, orange when only PduCDE is saturated, and in grey when neither enzyme is saturated. Red solid lines indicate when A_{cyto} is 1 μM; red dashed lines indicate when A_{cyto} is 10 nM. Black dashed lines indicate the baseline parameter values used in the model of the Pdu MCP.
(TIF)

Acknowledgments

Author Contributions

Conceptualization: CMJ MFS DTE NMM.

Funding acquisition: DTE.

Methodology: CMJ NMM.

Software: CMJ NMM.

Supervision: DTE NMM.

Writing – original draft: CMJ NMM.

Writing – review & editing: CMJ MFS DTE NMM.

References

1. Kerfeld CA, Heinhorst S, Cannon GC. Bacterial Microcompartments. Annu Rev Microbiol. 2010; 64: 391–408. https://doi.org/10.1146/annurev.micro.112408.134211 PMID: 20825353

2. Jorda J, Lopez D, Wheatley NM, Yeates TO. Using comparative genomics to uncover new kinds of protein-based metabolic organelles in bacteria. Protein Sci. 2013; 22: 179–195. https://doi.org/10.1002/pro.2196 PMID: 23188745

3. Axen SD, Erbilgin O, Kerfeld CA. A Taxonomy of Bacterial Microcompartment Loci Constructed by a Novel Scoring Method. Tanaka MM, editor. PLoS Comput Biol. 2014; 10: e1003898. https://doi.org/10.1371/journal.pcbi.1003898 PMID: 25340524

4.   Bobik TA, Havemann GD, Busch RJ, Williams DS, Aldrich HC. The Propanediol Utilization (pdu) Operon of *Salmonella enterica* Serovar Typhimurium LT2 Includes Genes Necessary for Formation of Polyhedral Organelles Involved in Coenzyme B12-Dependent 1, 2-Propanediol Degradation. J Bacteriol. 1999; 181: 5967–5975. PMID: 10498708

5.   Kofoid E, Rappleye C, Stojiljkovic I, Roth J. The 17-Gene Ethanolamine (eut) Operon of *Salmonella* typhimurium Encodes Five Homologues of Carboxysome Shell Proteins. J Bacteriol. 1999; 181: 5317–5329. PMID: 10464203

6.   Winter SE, Thiennimitr P, Winter MG, Butler BP, Huseby DL, Crawford RW, et al. Gut inflammation provides a respiratory electron acceptor for *Salmonella*. Nature. 2010; 467: 426–429. https://doi.org/10.1038/nature09415 PMID: 20864996

7.   Srikumar S, Fuchs TM. Ethanolamine Utilization Contributes to Proliferation of *Salmonella enterica* Serovar Typhimurium in Food and in Nematodes. Appl Environ Microbiol. 2010; 77: 281–290. https://doi.org/10.1128/AEM.01403-10 PMID: 21037291

8.   Bertin Y, Girardeau JP, Chaucheyras-Durand F, Lyan B, Pujos-Guillot E, Harel J, et al. Enterohaemorrhagic *Escherichia coli* gains a competitive advantage by using ethanolamine as a nitrogen source in the bovine intestinal content. Environ Microbiol. 2011; 13: 365–377. https://doi.org/10.1111/j.1462-2920.2010.02334.x PMID: 20849446

9.   Thiennimitr P, Winter SE, Winter MG, Xavier MN, Tolstikov V, Huseby DL, et al. Intestinal inflammation allows *Salmonella* to use ethanolamine to compete with the microbiota. Proc Natl Acad Sci. 2011; 108: 17480–17485. https://doi.org/10.1073/pnas.1107857108 PMID: 21969563

10.   Jakobson CM, Tullman-Ercek D. Dumpster Diving in the Gut: Bacterial Microcompartments as Part of a Host-Associated Lifestyle. PLOS Pathog. 2016; 12: e1005558. https://doi.org/10.1371/journal.ppat.1005558 PMID: 27171216

11.   Havemann GD, Sampson EM, Bobik TA. PduA is a shell protein of polyhedral organelles involved in coenzyme B12-dependent degradation of 1,2-propanediol in *Salmonella enterica* serovar Typhimurium LT2. J Bacteriol. 2002; 184: 1253–1261. https://doi.org/10.1128/JB.184.5.1253-1261.2002 PMID: 11844753

12.   Havemann GD, Bobik TA. Protein content of polyhedral organelles involved in coenzyme B12-dependent degradation of 1,2-propanediol in *Salmonella enterica* serovar Typhimurium LT2. J Bacteriol. 2003; 185: 5086–5095. https://doi.org/10.1128/JB.185.17.5086-5095.2003 PMID: 12923081

13.   Fan C, Cheng S, Liu Y, Escobar CM, Crowley CS, Jefferson RE, et al. Short N-terminal sequences package proteins into bacterial microcompartments. Proc Natl Acad Sci. 2010; 107: 7509–7514. https://doi.org/10.1073/pnas.0913199107 PMID: 20308536

14.   Fan C, Bobik TA. The N-terminal region of the medium subunit (PduD) packages adenosylcobalamin-dependent diol dehydratase (PduCDE) into the Pdu microcompartment. J Bacteriol. 2011; 193: 5623–5628. https://doi.org/10.1128/JB.05661-11 PMID: 21821773

15.   Fan C, Cheng S, Sinha S, Bobik TA. Interactions between the termini of lumen enzymes and shell proteins mediate enzyme encapsulation into bacterial microcompartments. Proc Natl Acad Sci. 2012; 109: 14995–15000. https://doi.org/10.1073/pnas.1207516109 PMID: 22927404

16.   Cheng S, Bobik TA. The PduQ Enzyme Is an Alcohol Dehydrogenase Used to Recycle NAD+ Internally within the Pdu Microcompartment of *Salmonella enterica*. 2012;

17.   Leal NA, Havemann GD, Bobik TA. PduP is a coenzyme-a-acylating propionaldehyde dehydrogenase associated with the polyhedral bodies involved in B 12-dependent 1, 2-propanediol degradation by *Salmonella enterica* serovar Typhimurium LT2. Arch Microbiol. 2003; 180: 353–361. https://doi.org/10.1007/s00203-003-0601-0 PMID: 14504694

18.   Cheng S. Recycling of vitamin B12 and NAD+ within the Pdu microcompartment of *enterica*. 2010; Available: http://lib.dr.iastate.edu/etd/11713/

19.   Huseby DL, Roth JR. Evidence that a metabolic microcompartment contains and recycles private cofactor pools. J Bacteriol. 2013; https://doi.org/10.1128/JB.02179-12 PMID: 23585538

20.   Price-Carter M, Tingey J, Bobik TA, Roth JR. The Alternative Electron Acceptor Tetrathionate Supports B12-Dependent Anaerobic Growth of *Salmonella enterica* Serovar Typhimurium on Ethanolamine or 1,2-Propanediol. J Bacteriol. 2001; 183: 2463–2475. https://doi.org/10.1128/JB.183.8.2463-2475.2001 PMID: 11274105

21.   Sampson EM, Bobik TA. Microcompartments for B12-Dependent 1,2-Propanediol Degradation Provide Protection from DNA and Cellular Damage by a Reactive Metabolic Intermediate. J Bacteriol. 2008; 190: 2966–2971. https://doi.org/10.1128/JB.01925-07 PMID: 18296526

22.   Mangan NM, Brenner MP. Systems analysis of the CO2 concentrating mechanism in cyanobacteria. eLife. 2014; 3: e02043. https://doi.org/10.7554/eLife.02043

23. Schaechter M, MaalØe O, Kjeldgaard NO. Dependency on Medium and Temperature of Cell Size and Chemical Composition during Balanced Growth of *Salmonella* typhimurium. Microbiology. 1958; 19: 592–606.

24. Jakobson CM, Chen Y, Slininger MF, Valdivia E, Kim EY, Tullman-Ercek D. Tuning the Catalytic Activity of Subcellular Nanoreactors. J Mol Biol. PMID: 27427532

25. Chen P, Andersson DI, Roth JR. The control region of the pdu/cob regulon in *Salmonella* typhimurium. J Bacteriol. 1994; 176: 5474–5482. https://doi.org/10.1128/jb.176.17.5474-5482.1994 PMID: 8071226

26. Dueber JE, Wu GC, Malmirchegini GR, Moon TS, Petzold CJ, Ullal AV, et al. Synthetic protein scaffolds provide modular control over metabolic flux. Nature biotechnology. 2009; 27: 753–759. https://doi.org/10.1038/nbt.1557 PMID: 19648908

27. Delebecque CJ, Lindner AB, Silver PA, Aldaye FA. Organization of Intracellular Reactions with Rationally Designed RNA Assemblies. Science. 2011; 333: 470–474. https://doi.org/10.1126/science.1206938 PMID: 21700839

28. Conrado RJ, Mansell TJ, Varner JD, DeLisa MP. Stochastic reaction–diffusion simulation of enzyme compartmentalization reveals improved catalytic efficiency for a synthetic metabolic pathway. Metab Eng. 2007; 9: 355–363. https://doi.org/10.1016/j.ymben.2007.05.002 PMID: 17601761

29. Narayanaswamy R, Levy M, Tsechansky M, Stovall GM, O'Connell JD, Mirrielees J, et al. Widespread reorganization of metabolic enzymes into reversible assemblies upon nutrient starvation. PNAS. 2009; 106: 10147–10152. https://doi.org/10.1073/pnas.0812771106 PMID: 19502427

30. Zhao A, Tsechansky M, Ellington A D., Marcotte E M.. Revisiting and revising the purinosome. Molecular BioSystems. 2014; 10: 369–374. https://doi.org/10.1039/c3mb70397e PMID: 24413256

31. Castellana M, Wilson MZ, Xu Y, Joshi P, Cristea IM, Rabinowitz JD, et al. Enzyme clustering accelerates processing of intermediates through metabolic channeling. Nat Biotech. 2014; 32: 1011–1018. https://doi.org/10.1038/nbt.3018

32. Mangan NM, Flamholz A, Hood RD, Milo R, Savage DF. pH determines the energetic efficiency of the cyanobacterial CO2 concentrating mechanism. PNAS. 2016; 113: E5354–E5362. https://doi.org/10.1073/pnas.1525145113 PMID: 27551079

33. Faber F, Thiennimitr P, Spiga L, Byndloss MX, Litvak Y, Lawhon S, et al. Respiration of Microbiota-Derived 1,2-propanediol Drives Salmonella Expansion during Colitis. PLOS Pathogens. 2017; 13: e1006129. https://doi.org/10.1371/journal.ppat.1006129 PMID: 28056091

34. Chowdhury C, Chun S, Pang A, Sawaya MR, Sinha S, Yeates TO, et al. Selective molecular transport through the protein shell of a bacterial microcompartment organelle. Proc Natl Acad Sci. 2015; 201423672. https://doi.org/10.1073/pnas.1423672112 PMID: 25713376

35. Glasgow JE, Asensio MA, Jakobson CM, Francis MB, Tullman-Ercek D. Influence of Electrostatics on Small Molecule Flux through a Protein Nanoreactor. ACS Synth Biol. 2015; https://doi.org/10.1021/acssynbio.5b00037 PMID: 25893987

36. Lee H, DeLoache WC, Dueber JE. Spatial organization of enzymes for metabolic engineering. Metab Eng. 2012; 14: 242–251.

37. Mastro AM, Babich MA, Taylor WD, Keith AD. Diffusion of a small molecule in the cytoplasm of mammalian cells. Proc Natl Acad Sci. 1984; 81: 3414–3418. https://doi.org/10.1073/pnas.81.11.3414 PMID: 6328515

38. Robertson RN. Lively Membranes. CUP Archive; 1983.

39. Bachovchin WW, Eagar RG, Moore KW, Richards JH. Mechanism of action of adenosylcobalamin: glycerol and other substrate analogs as substrates and inactivators for propanediol dehydratase—kinetics, stereospecificity, and mechanism. Biochemistry (Mosc). 1977; 16: 1082–1092. https://doi.org/10.1021/bi00625a009